

Western University

Scholarship@Western

Chemistry Publications

Chemistry Department

6-6-2018

Effects of Dispersion Corrections and Nonlocality on Density Functional Predictions of Pressure-Induced Polymorphic Transitions of Crystalline Diborane

Angela M. Murcia Rios

Darya N. Komsa

Viktor N. Staroverov

Follow this and additional works at: <https://ir.lib.uwo.ca/chempub>

 Part of the [Chemistry Commons](#)

1
2
3 **Effects of Dispersion Corrections and Nonlocality on**
4
5 **Density-Functional Predictions of Pressure-Induced Polymorphic**
6
7 **Transitions of Crystalline Diborane**
8
9

10 Angela M. Murcia Rios, Darya N. Komsa, and Viktor N. Staroverov

11 *Department of Chemistry, The University of Western Ontario,*

12 *London, Ontario N6A 5B7, Canada*
13

14
15
16 (Dated: May 30, 2018)
17

18 **Abstract**
19

20 The role of dispersion interactions in density-functional calculations of the relative enthalpies
21 of compressed BH_3 polymorphs was investigated using plane-wave and Gaussian-basis-set codes.
22 Inclusion of semiempirical atom-pairwise dispersion corrections was found to have little effect on
23 the relative enthalpies of various boron hydride structures. By contrast, the stability ranking
24 obtained with the nonlocal van der Waals density functional (vdW-DF) of Dion and co-workers
25 was substantially more realistic than that predicted by generalized gradient approximations. Of
26 the functionals tested, only vdW-DF correctly predicts that compressed diborane does not leave
27 the B_2H_6 motif until at least 20 GPa. This finding serves as direct computational evidence of the
28 thermodynamic stability of molecular B_2H_6 units in the 0–20 GPa pressure range, an experimental
29 result that until now has been at variance with theoretical predictions.
30
31
32
33
34
35
36
37
38
39
40
41
42
43
44
45
46
47
48
49
50
51
52
53
54
55
56
57
58
59
60

INTRODUCTION

Density-functional theory (DFT) is the main tool for studying the structure and properties of materials whose experimental characterization is challenging. This is particularly true for materials under extreme pressures. High-pressure boron hydrides obtained by compressing molecular crystals of diborane (B_2H_6) are notable in that regard as possible energy-storage materials and high-temperature superconductors.¹⁻⁷

To date, only one crystalline structure of boron hydride, the so-called β -phase consisting of B_2H_6 molecules, has been completely characterized by X-ray diffraction.^{8,9} Structures of several other polymorphs have been inferred by comparing experimental^{1,2} and simulated^{10,11} vibrational spectra. Such indirect evidence suggests that β -diborane undergoes a sequence of polymorphic transitions near 6, 14, 42, and 57 GPa, and that all of the phases involved consist of differently packed B_2H_6 units.^{10,11}

According to density-functional calculations, however, molecular crystals of B_2H_6 are not the most thermodynamically stable phase of compressed boron hydride. Yao and Hoffmann¹² calculated relative enthalpies of ten diverse BH_3 polymorphs using the Perdew–Burke–Ernzerhof¹³ (PBE) functional and concluded that the B_2H_6 units of solid diborane should transform near 4 GPa into trimers, $(BH_3)_3$, and then near 36 GPa into one-dimensional polymeric chains which should remain stable until at least 100 GPa. Similar conclusions were reached by Torabi *et al.*¹⁰ who employed the PBE functional for solids¹⁴ (PBEsol). Above 100 GPa, the most stable phase of boron hydride was predicted to consist of three-dimensional B–B and B–H bond networks.^{4,5}

The apparent inconsistency between theory and experiment has been attributed to the kinetic stability of molecular B_2H_6 crystals.¹⁰ Another possible factor is neglect of the dispersion interactions by the PBE and PBEsol functionals, at least for low-pressure structures. The role of dispersion interactions can be crucial in predictions of relative enthalpies of molecular and covalent crystals.¹⁵⁻¹⁹ In this work, we examine how the inclusion of dispersion corrections and the use of fully nonlocal correlation functionals affect the predicted stability of diverse BH_3 polymorphs.

DISPERSION CORRECTIONS

Most density-functional approximations including the local density approximation (LDA) and generalized gradients approximations (GGA) such as PBE¹³, PBEsol¹⁴ and revised PBE²⁰ (revPBE) do not account for dispersion interactions. In order to describe those noncovalent interactions, two approaches are commonly used: semiempirical dispersion corrections, which are applied to total electronic energies obtained by self-consistent Kohn–Sham calculations, and nonlocal correlation functionals, which incorporate dispersion interactions by construction. In this work we test both approaches: the former is represented by Grimme’s DFT-D^{21–24} dispersion correction schemes and by the Becke–Johnson exchange–hole dipole moment^{25–28} (XDM) model, the latter by the nonlocal van der Waals density functional (vdW-DF) of Dion and co-workers.²⁹

DFT-D2 and DFT-D3 are particular implementations of the DFT-D scheme. In the DFT-D2 method,²¹ the dispersion energy is written as

$$E_{\text{disp}}^{\text{D2}} = - \sum_{\text{A}<\text{B}} s_6 \frac{C_6^{\text{AB}}}{R_{\text{AB}}^6} f_{\text{damp}}(R_{\text{AB}}) \quad (1)$$

where R_{AB} is the internuclear distance between atoms A and B, $f_{\text{damp}}(R_{\text{AB}})$ is a damping function, C_6^{AB} is the averaged 6th-order dispersion coefficient for the AB pair, and s_6 is a functional-dependent global scaling factor. The C_6^{AB} coefficients are computed as the geometric mean of C_6^{AA} and C_6^{BB} , which in turn are determined by fitting. The damping function $f_{\text{damp}}(R_{\text{AB}})$ is introduced to avoid singularities arising as $R_{\text{AB}} \rightarrow 0$. Several forms of this function have been proposed, all such that each AB-pair contribution to $E_{\text{disp}}^{\text{D2}}$ vanishes as $R_{\text{AB}} \rightarrow 0$.²³

DFT-D3²² is a refinement of the DFT-D2 scheme. It incorporates both the C_6 and C_8 terms (computed from first principles in the DFT-D3 scheme) and explicitly takes into account molecular environment through the empirical concept of fractional coordination numbers. According to the DFT-D2 and DFT-D3 schemes, dispersion-energy contributions from closest-neighbor atoms should vanish in highly compressed structures because internuclear distances in such structures eventually drop below the built-in cutoffs.

In the XDM model, the dispersion energy is given by²⁷

$$E_{\text{disp}}^{\text{XDM}} = - \sum_{\text{A}<\text{B}} \sum_{n=6,8,10} \frac{C_n^{\text{AB}}}{R_{\text{AB}}^n + a_{\text{AB}}^n} \quad (2)$$

where the coefficients C_n^{AB} are calculated on the fly from the exchange-hole multipole moments and static polarizabilities of atoms A and B, and a_{AB}^n are parameters. Thus, XDM corrections are density-dependent, whereas DFT-D2 corrections are determined solely by nuclear positions.

A version of the DFT-D3 method which uses the Becke–Johnson-type damping²⁷ is referred to as DFT-D3BJ,^{23,24}

$$E_{\text{disp}}^{\text{D3BJ}} = - \sum_{A<B} \sum_{n=6,8} \frac{C_n^{AB}}{R_{AB}^n + (a_1 R_{AB}^0 + a_2)^n} \quad (3)$$

where $R_{AB}^0 = \sqrt{C_8^{AB}/C_6^{AB}}$ and where a_1 and a_2 are parameters.

The analytic form of Eqs. (2) and (3) is such that individual AB contributions to $E_{\text{disp}}^{\text{XDM}}$ and $E_{\text{disp}}^{\text{D3BJ}}$ do not vanish as $R_{AB} \rightarrow 0$ but rather approach an AB-dependent constant. This means that XDM and D3BJ corrections will be nonzero for closest-neighbor atoms even in highly compressed structures.

The vdW-DF method of Dion and co-workers²⁹ is conceptually different from the DFT-D and XDM schemes in that the dispersion energy is not an add-on but is incorporated into the functional. The vdW-DF approximation is the revPBE exchange-correlation GGA in which the PBE gradient correction for correlation has been replaced with a nonlocal (NL) functional

$$E_C^{\text{NL}}[\rho] = \frac{1}{2} \int d\mathbf{r} \int d\mathbf{r}' \rho(\mathbf{r}) \phi(\mathbf{r}, \mathbf{r}') \rho(\mathbf{r}') \quad (4)$$

where the function $\phi(\mathbf{r}, \mathbf{r}')$ depends on the density, its gradient, and $|\mathbf{r} - \mathbf{r}'|$. The entire vdW-DF approximation therefore has the form

$$E^{\text{vdW-DF}}[\rho] = E_X^{\text{revPBE}}[\rho] + E_C^{\text{LDA}}[\rho] + E_C^{\text{NL}}[\rho] \quad (5)$$

Even the simplest of the dispersion correction schemes considered in this work, DFT-D2, significantly improves the accuracy of thermodynamic predictions for weakly bonded complexes and molecular crystals.^{21,24,30–32} The DFT-D3, DFT-B3BJ, and XDM methods outperform DFT-D2,^{24,30–32} and the vdW-DF approximation has been reported to work even better for molecular complexes.²⁴

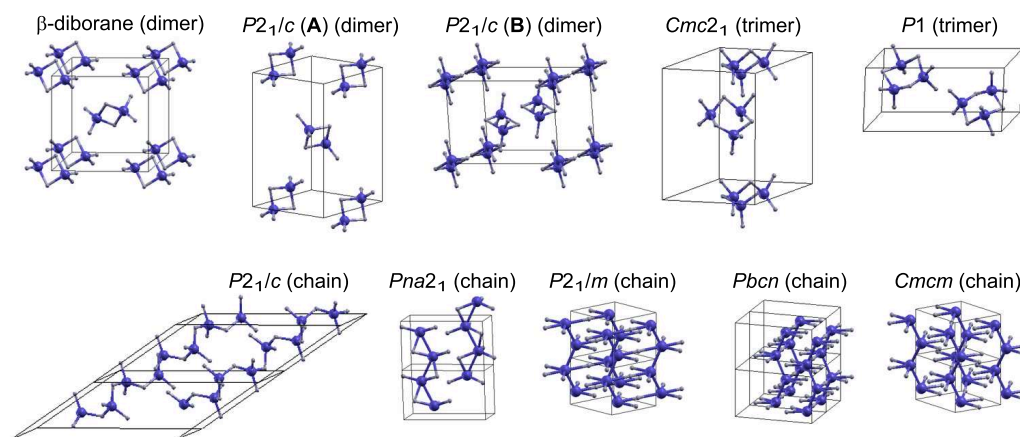
Dispersion corrections are expected to be more important for solids at ambient pressures than for highly compressed structures. One may even wonder whether it makes sense to apply the semiempirical DFT-D and XDM schemes, which were designed and parametrized

1
2
3 for normal internuclear distances, to compressed crystals where interatomic repulsion is
4 much greater than dispersion energy. Nevertheless, we are going to apply the DFT-D and
5 XDM methods anyway even at pressures as high as 100 GPa, if only to test how robust
6 these scheme are with respect to bond compression.
7
8
9

METHODOLOGY

10
11
12
13
14
15 The ambient-pressure structures of the ten BH_3 polymorphs examined in this work are
16 shown in Figure 1. These are the same structures that were investigated in ref 10. The
17 designations “dimer” and “trimer” refer to the molecular units existing at ambient pressure.
18 Some of these structures polymerize at $P > 50$ GPa, but we will continue to label them as
19 “dimers” and “trimers” to avoid confusion. Each structure was optimized by minimizing the
20 enthalpy at a given pressure with the total electronic energy obtained using the following
21 approximations: PBEsol, PBEsol-D2, PBEsol-XDM, PBE, PBE-D3BJ, revPBE, revPBE-
22 XDM, and vdW-DF. The PBEsol functional differs from PBE and revPBE in that it is
23 designed to become asymptotically exact for solids under extreme compression,^{14,33} which is
24 why it was chosen for this study.
25
26
27
28
29
30
31

32 All plane-wave calculations were performed using the Quantum ESPRESSO³⁴ package,
33 Release 5.1.1, with a kinetic energy cutoff set to 100 Ry. The Monkhorst–Pack³⁵ \mathbf{k} -mesh was
34 used for Brillouin zone sampling (see Table S1 in the Supporting Information for details).
35 The energy threshold for the convergence of self-consistent-field cycles was 10^{-10} Ry. All lat-
36
37
38
39



56 Figure 1: The ten ambient-pressure structures of crystalline boron hydride studied in this work.
57
58
59
60

1
2
3 tice structures were optimized using the Broyden–Fletcher–Goldfarb–Shanno quasi-Newton
4 algorithm with a 10^{-4} Ry/Å threshold for the Hellmann–Feynman forces and 10^{-5} Ry for
5 the total energy. The pressure on the cell upon convergence was within 0.05 GPa of the
6 target value.
7
8
9

10 We used PBE ultrasoft pseudopotentials³⁶ for all methods except PBEsol-XDM, for
11 which we had to resort to projected-augmented-wave (PAW) revPBE pseudopotentials,^{37,38}
12 the only option available for the XDM scheme in the Quantum ESPRESSO release used.
13 All pseudopotentials were taken from the Quantum ESPRESSO pseudopotential library.³⁹
14 To test the adequacy of ultrasoft pseudopotentials for highly compressed BH₃ polymorphs
15 (cf. ref 40), we performed revPBE geometry optimizations for each of the 10 structures
16 in the 10–100 GPa pressure range using three types of pseudopotentials: ultrasoft, PAW,
17 and norm-conserving (all PBE-based). The discrepancies between the relative enthalpies ob-
18 tained using the PAW and ultrasoft pseudopotentials did not exceed 0.011 eV at any pressure.
19 The discrepancies between the relative enthalpies obtained using the norm-conserving and
20 ultrasoft pseudopotentials were under 0.008 eV for the oligomers and mostly under 0.020
21 eV for the chains; the largest discrepancy was 0.024 eV for the *Pbcn* chains at 50 and 100
22 GPa. Such discrepancies are insignificant for the purposes of this study.
23
24
25
26
27
28
29
30
31
32

33 Calculations using the *Gaussian 09* program⁴¹ were carried out using the ultrafine inte-
34 gration grid, automatically generated density fitting sets, and default **k**-meshes.
35

36 All reported enthalpies are for 0 K and do not include the vibrational zero-point energies
37 (ZPE) in order to facilitate comparison with previous^{10–12} and future DFT studies. Yao
38 and Hoffmann¹² showed that the ZPEs of diverse gas-phase isomers of (BH₃)_n with $n = 2–4$
39 differ by no more than 0.025 eV/BH₃, and we assume here that the *differences* between the
40 ZPEs of the polymorphs shown in Figure 1 do not exceed 0.1 eV/BH₃. The main conclusion
41 of this work is predicated on that assumption.
42
43
44
45
46
47
48

49 RESULTS AND DISCUSSION

50
51 The shortest intermolecular (interchain) distance between atoms generally decreases with
52 increasing pressure (Figure 2), as do intramolecular bonds.⁴² In the *P2₁/c* (**A**) structure,
53 the shortest intermolecular distance becomes intramolecular when the B₂H₆ units form a
54 polymeric chain between 50 and 100 GPa, so the minimal R_{BB} values at $P = 50$ GPa and
55
56
57
58
59
60

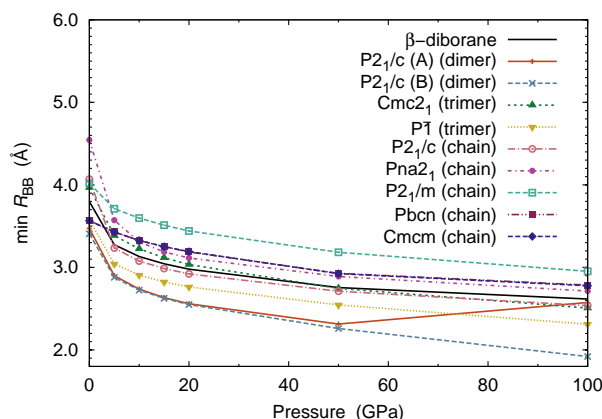


Figure 2: The shortest intermolecular (interchain) distances between B atoms in PBEsol structures as a function of pressure.

$P = 100$ GPa are for different pair of atoms. This switch-over explains the apparent increase in the smallest R_{BB} distance observed above 50 GPa.

At short internuclear distances, the DFT-D and XDM methods damp the corresponding dispersion-energy term and, in the case of DFT-D2 and DFT-D3 schemes, may turn it off completely when the atoms are separated by less than 1 Å. This means that, at sufficiently high pressures, dispersion corrections between some pairs of atoms may be almost completely damped. This should be kept in mind when one applies semiempirical dispersion corrections to all compressed solids.

According to our interpretation¹⁰ of the experimental vibrational spectra^{1,2} of compressed diborane, β -diborane transforms into a $P2_1/c$ (**A**) dimer-based structure near 6 GPa and then into another dimer-based polymorph, $P2_1/c$ (**B**), near 14 GPa. Let us see to what extent these transformations are predicted by various density-functional approximations.

Plane-wave calculations

Consider first the uncorrected PBEsol results (Figure 3a). At 0 GPa, the stability ranking of the dimer- and trimer-based structures predicted by PBEsol is

$$Cmc2_1 \approx P\bar{1} < \beta\text{-diborane} \approx P2_1/c \text{ (A)} \approx P2_1/c \text{ (B)}$$

(trimer) (trimer) (dimer) (dimer) (dimer)

This is in slight disagreement with experiment¹⁰ and with PBE,¹² both of which predict β -diborane to be the most stable forms at ambient pressure (recall that PBE is a better

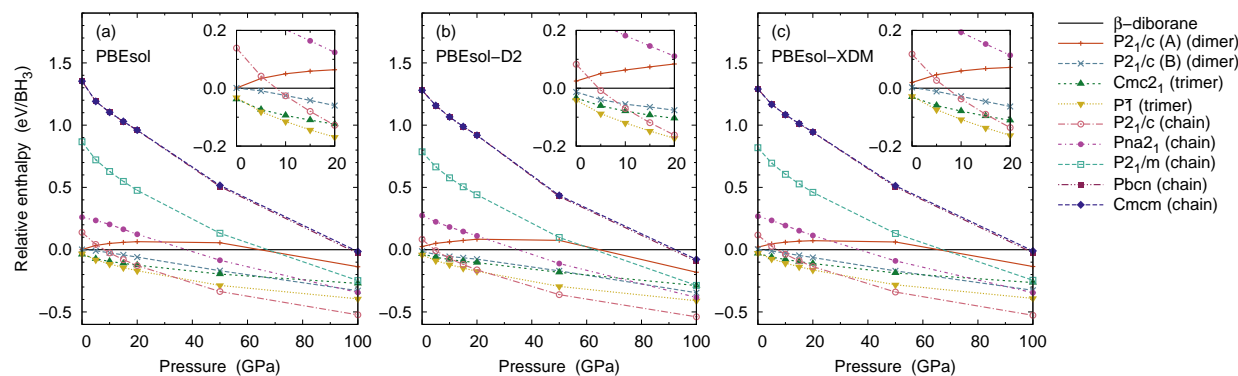


Figure 3: Enthalpies of the ten crystalline boron hydride structures of Figure 1 relative to β -diborane: (a) without dispersion corrections; (b) and (c) with dispersion corrections. The data plotted may be found in Table S2 of the Supporting Information.

functional than PBEsol for computing energies at ambient pressures). At 5 GPa, PBEsol predicts the following order

$$\begin{matrix} P\bar{1} & \approx & Cmc2_1 & < & P2_1/c & (\mathbf{B}) & \approx & \beta\text{-diborane} & < & P2_1/c & (\mathbf{A}) \\ (\text{trimer}) & & (\text{trimer}) & & (\text{dimer}) & & (\text{dimer}) & & (\text{dimer}) & & (\text{dimer}) \end{matrix}$$

which is largely in agreement with PBE¹² but still at variance with experiment. Polymeric $(\text{BH}_3)_n$ chains are thermodynamically unstable at 0 GPa according to both PBEsol and PBE. As the pressure increases, PBEsol enthalpies of the chain structures decrease faster than those of the dimers and trimers, and around 30 GPa the $P2_1/c$ chain structure becomes the most stable (PBE and PBEsol agree on that).

The PBEsol-D2 method predicts practically the same stability rankings as PBEsol for the three lowest-enthalpy structures at 0 and 5 GPa (Figure 3b). The average effect of adding dispersion corrections to the PBEsol enthalpies does not exceed 0.05 eV per BH_3 unit (Table S2). Overall, the D2 correction to PBEsol is not sufficient to change the stability rankings substantially at any pressure in the 0–100 GPa range. The XDM correction makes even less difference than DFT-D: the PBEsol and PBEsol-XDM relative enthalpies are barely distinguishable at most pressures (Figure 3c).

Note that because PBEsol has a smaller enhancement factor than PBE and most other GGAs, it is sometimes not the best GGA to pair up with semiempirical dispersion corrections.⁴³ To check whether our choice of PBEsol might have impaired the XDM model, we also applied the XDM scheme to a “normal” GGA, revPBE. Comparison of Figures

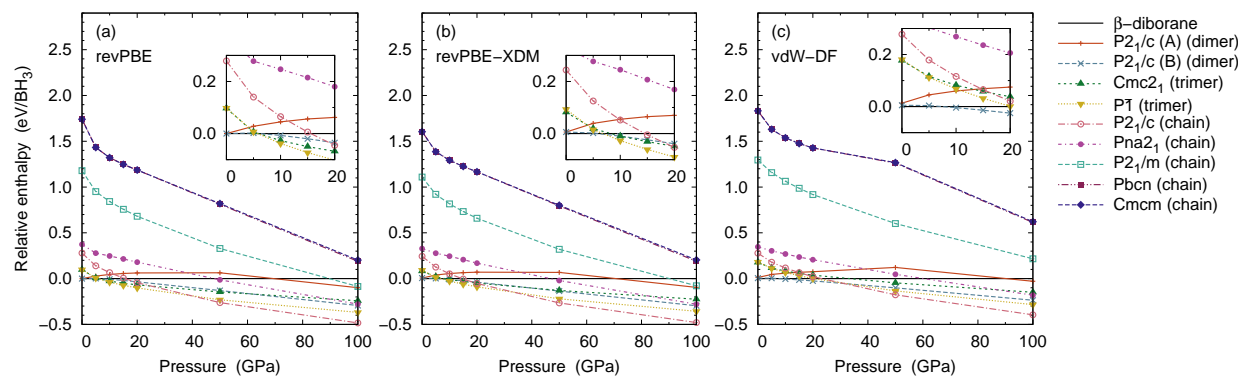


Figure 4: Enthalpies of the ten crystalline boron hydride structures of Figure 1 relative to β -diborane: (a) revPBE without dispersion (b) revPBE with XDM dispersion corrections; (c) vdW-DF (revPBE with a nonlocal correlation functional). The data plotted may be found in Table S3 of the Supporting Information.

4a and 4b shows that the XDM correction has no appreciable effect on the revPBE enthalpies, as was the case with PBEsol. Thus, the use of PBEsol as a base functional does not disadvantage the semiempirical dispersion schemes in the context of this work.

Now consider the revPBE and vdW-DF (dispersion-corrected revPBE) results (Figures 4a and 4c). At 0 GPa, the stability ranking of the dimer- and trimer-based structures predicted by revPBE and vdW-DF is

$$\beta\text{-diborane} \approx P2_1/c \text{ (A)} \approx P2_1/c \text{ (B)} < P\bar{1} \approx Cmc2_1$$

(dimer) (dimer) (dimer) (trimer) (trimer)

According to revPBE and vdW-DF, β -diborane remains the lowest-enthalpy structure until 6–7 GPa, which is in agreement with experiment.¹⁰ At 10 GPa, the revPBE ranking changes to

$$P\bar{1} \approx Cmc2_1 < P2_1/c \text{ (B)} \approx \beta\text{-diborane} < P2_1/c \text{ (A)}$$

(trimer) (trimer) (dimer) (dimer) (dimer)

whereas the vdW-DF ranking is

$$P2_1/c \text{ (B)} \approx \beta\text{-diborane} < P2_1/c \text{ (A)} \approx P\bar{1} \approx Cmc2_1$$

(dimer) (dimer) (dimer) (trimer) (trimer)

Throughout the 7–20 GPa range, revPBE predicts the two trimer structures to be the most stable (PBE makes a similar prediction¹²), which is at odds with experiment. But vdW-DF identifies one of the dimer-based polymorphs, $P2_1/c \text{ (B)}$, as the lowest-enthalpy structure from 7 to at least 20 GPa. This prediction is not perfect because, experimentally, the

1
2
3 $P2_1/c$ (**B**) structure becomes the most stable one only near 14 GPa.¹⁰ However, this is the
4 first computational evidence that the B_2H_6 units remain intact in the 0–20 GPa pressure
5 range. The revPBE and vdW-DF stability rankings continue to differ substantially at higher
6 pressures, although they both agree that the $(BH_3)_n$ chains become more stable than the
7 dimer-based structures above 40 GPa.
8
9

10
11 Note that the relative enthalpies shown in Figures 3 and 4 are for the respective opti-
12 mized geometries. To quantify the effect of geometry relaxation on these predictions, we
13 also computed PBEsol-D2 and PBEsol-XDM relative enthalpies for the PBEsol-optimized
14 structures, as well as vdW-DF relative enthalpies for the revPBE-optimized structures. The
15 results were on average within 0.01 eV/ BH_3 of those for the relaxed geometries (Tables S2
16 and S3), which indicates that the change in the stability rankings seen in Figures 3 and 4
17 are almost exclusively due to the inclusion of dispersion interactions.
18
19
20
21
22
23
24
25

26 **Gaussian-basis-set calculations**

27
28
29 The *Gaussian 09*⁴¹ program offers a wide selection of density-functional approximations
30 which can be combined with Grimme’s dispersion corrections. Unlike Quantum ESPRESSO,
31 it uses localized Gaussian-type basis functions to represent the Kohn–Sham orbitals. Com-
32 parison of all-electron Gaussian-basis-set calculations with plane-wave calculations employ-
33 ing pseudopotentials can therefore provide an additional validation of our conclusions.
34
35

36 First, we set out to determine which Gaussian basis set affords the best agreement with
37 plane-wave calculations on boron hydrides. To this end, we took the optimized PBE geome-
38 tries of the ten periodic structures shown in Figure 1 and used the *Gaussian 09* program to
39 recompute their PBE energies (without any dispersion corrections) at ambient pressure (1
40 atm \approx 0 GPa) using various Gaussian basis sets. The basis sets we tested include D95V,
41 6-31G*, 6-311G*, 6-311G**, cc-pVDZ, cc-pVTZ, TZV, and TZVP. The best agreement was
42 obtained for the 6-311G** and TZVP basis sets (Table 1). We have also tested the 6-311+G*
43 basis set and found that it gives the same PBE energies as the 6-311G* within 0.01 eV/ BH_3 .
44 This indicates that diffuse functions are not essential in calculations on crystalline boron
45 hydrides. Based on these findings, we adopted the 6-311G** basis set for further studies.
46
47
48
49
50
51
52
53
54

55 At zero temperature and pressure ($T = 0$, $P = 0$), the enthalpy H of a system is equal
56 to its internal energy E . At $P \gg 0$, the enthalpy of crystals can no longer be equated with
57
58
59
60

Table 1: Relative PBE Enthalpies (eV/BH₃) of Various BH₃ Polymorphs Calculated Using Plane-Wave (PW) and Gaussian Basis Sets ($P = 0$ GPa)

Structure	PW ^a	Gaussian basis sets							
		D95V	6-31G*	6-311G*	6-311G**	cc-pVDZ	cc-pVTZ	TZV	TZVP
β -diborane (dimer)	0.000	0.000	0.000	0.000	0.000	0.000	0.000	0.000	0.000
$P2_1/c$ (A) (dimer)	0.002	0.006	0.003	0.004	0.003	0.004	0.003	0.009	0.003
$P2_1/c$ (B) (dimer)	0.002	0.001	0.001	-0.001	0.000	0.000	0.000	0.000	0.000
$Cmc2_1$ (trimer)	0.114	0.023	0.062	0.058	0.053	0.032	0.055	0.068	0.055
$P\bar{1}$ (trimer)	0.045	0.026	0.059	0.052	0.049	0.031	0.051	0.070	0.050
$P2_1/c$ (chain)	0.209	0.158	0.222	0.215	0.212	0.191	0.215	0.220	0.216
$Pna2_1$ (chain)	0.308	0.254	0.325	0.310	0.311	0.290	0.314	0.321	0.315
$P2_1/m$ (chain)	1.034	1.192	1.222	1.127	1.044	1.010	1.045	1.196	1.048
$Pbcn$ (chain)	1.547	1.580	1.733	1.635	1.552	1.475	1.564	1.609	1.559
$Cmcm$ (chain)	1.537	1.586	1.738	1.641	1.556	1.478	1.568	1.617	1.563
MAD ^b		0.046	0.067	0.036	0.011	0.029	0.014	0.041	0.013

^aWith PBE ultrasoft pseudopotentials.

^bMean absolute deviation with respect to the PW values.

E even for $T = 0$, and the relation $H = E + pV$ must be used. By combining the total electronic energy predicted by *Gaussian 09* with the pV term we were able to show that PBE/6-311G** enthalpies agree well with the corresponding plane-wave PBE enthalpies even at high pressures (Table 2).

To assess the significance of dispersion corrections in Gaussian-basis-set calculations on BH₃ polymorphs, we chose to use the PBE functional and the DFT-D3BJ dispersion correction scheme. Because dispersion corrections are not available for periodic systems in the *Gaussian 09* release we used, we modeled the crystals with finite clusters. Each of the clusters consisted of 27 ($3 \times 3 \times 3$) units cells arranged along the crystallographic axes with the same lattice constants as in the crystals optimized at 0 GPa by the plane-wave PBE method. Due to the relatively large size of these clusters, dispersion-corrected DFT calculations using the 6-311G** basis set proved to be too expensive, so we employed the 6-31G* basis set instead. This basis set is suboptimal (Table 1) but was presumed sufficient to estimate the

Table 2: Relative PBE Energies and Enthalpies (eV/BH₃) of Selected BH₃ Polymorphs Calculated Using the 6-311G** and PW Basis Sets ($P = 50$ GPa)

Structure ^a	6-311G**			PW
	ΔE	$p\Delta V$	ΔH	ΔH
β -diborane (dimer)	0.000	0.000	0.000	0.000
$P2_1/c$ (A) (dimer)	0.115	-0.059	0.056	0.120
$P2_1/c$ (B) (dimer)	0.013	-0.162	-0.149	-0.137
$Cmc2_1$ (trimer)	-0.030	-0.130	-0.160	-0.146
$Pna2_1$ (chain)	0.258	-0.301	-0.043	-0.031
$P2_1/m$ (chain)	0.774	-0.503	0.272	0.267
$Pbcn$ (chain)	1.392	-0.636	0.757	0.744
$Cmcm$ (chain)	1.575	-0.839	0.737	0.883

^aThe 6-311G** results are for the PBE/PW structures.

Table 3: Relative PBE/6-31G* and PBE-D3BJ/6-31G* Energies (eV/BH₃) of 27-Unit-Cell Clusters Representing Selected BH₃ Polymorphs ($P = 0$ GPa)

Structure	PBE	PBE+D3BJ
β -diborane	0.000	0.000
$P2_1/c$ (A) (dimer)	0.001	0.002
$P2_1/c$ (B) (dimer)	-0.002	-0.005
$Cmc2_1$ (trimer)	0.062	0.032
$P\bar{1}$ (trimer)	0.058	0.037

magnitude of dispersion energies. From the data obtained for the dimer- and trimer-based structures (Table 3) it is clear that the effect of the D3BJ dispersion correction on PBE energies is insignificant. This is consistent with the results of plane-wave calculations using the DFT-D scheme.

CONCLUSION

We have investigated how inclusion of dispersion energy through the DFT-D, XDM, and vdW-DF schemes influences relative GGA enthalpies of various BH_3 polymorphs. The DFT-D2 and XDM schemes affect the relative enthalpies only slightly and, except for a few cases of almost degenerate structures, do not alter the polymorph stability rankings predicted by PBE, PBEsol, and revPBE. By contrast, vdW-DF was found to perform qualitatively better than those GGAs. Results of all-electron DFT-D3BJ Gaussian-basis-set calculations on finite clusters of B_2H_6 and B_3H_9 molecules are consistent with these conclusions.

The most significant finding of this work is that the nonlocal vdW-DF approximation predicts that compressed diborane does not leave the B_2H_6 motif until at least 20 GPa, in agreement with experiment. No GGA employed in this work or elsewhere^{10–12} has been able to predict this outcome. The vdW-DF approximation also properly identifies the $P2_1/c$ (**B**) structure as the most stable polymorph in the 14–20 GPa range, even though it still assigns a relatively high enthalpy to the $P2_1/c$ (**A**) structure, another dimer-based polymorph that is believed¹⁰ to be the most stable phase between 6 and 14 GPa.

When rationalizing the better performance of the vdW-DF approximation one should keep in mind that vdW-DF is a nonlocal functional, whereas the PBE, PBEsol, and revPBE are all semilocal. Therefore, the success of vdW-DF should be attributed in part to the more accurate description of electron correlation as a whole. It should also be noted that the calculations of this work do not include ZPEs, thermal corrections, or many-body dispersion terms. Such contributions can be essential in predictions of the relative enthalpies of crystal polymorphs,^{18,19,44–48} and their significance for computational studies of various BH_3 phases remains to be investigated.

Supporting Information

Specification of **k**-point meshes used in the plane-wave calculations; enthalpies of individual crystalline boron hydride structures (relative to β -diborane) calculated using the PBEsol, PBEsol-D2, PBE-XDM, revPBE, revPBE-XDM, and vdW-DF approximations.

Acknowledgments

The authors thank Prof. Yang Song for helpful comments on the manuscript. The work was supported by the Natural Sciences and Engineering Research Council of Canada (NSERC) through the Discovery Grants program (RGPIN-2015-04814 and RGPAS 477791-2015).

References

- 1 Murli, C.; Song, Y. Pressure-Induced Transformations in Diborane: A Raman Spectroscopic Study. *J. Phys. Chem. B* **2009**, *113*, 13509–13515.
- 2 Song, Y.; Murli, C.; Liu, Z. *In Situ* High-Pressure Study of Diborane by Infrared Spectroscopy. *J. Chem. Phys.* **2009**, *131*, 174506.
- 3 Song, Y. New Perspectives on Potential Hydrogen Storage Materials Using High Pressure. *Phys. Chem. Chem. Phys.* **2013**, *15*, 14524–14547.
- 4 Abe, K.; Ashcroft, N. W. Crystalline Diborane at High Pressures. *Phys. Rev. B* **2011**, *84*, 104118.
- 5 Hu, C.-H.; Oganov, A. R.; Zhu, Q.; Qian, G.-R.; Frapper, G.; Lyakhov, A. O.; Zhou, H.-Y. Pressure-Induced Stabilization and Insulator-Superconductor Transition of BH. *Phys. Rev. Lett.* **2013**, *110*, 165504.
- 6 Szcześniak, R.; Drzazga, E. A.; Duda, A. M. The Superconducting State in the B₂H₆ Compound at 360 GPa. *Solid State Commun.* **2013**, *166*, 50–55.
- 7 Duan, D.; Liu, Y.; Ma, Y.; Shao, Z.; Liu, B.; Cui, T. Structure and Superconductivity of Hydrides at High Pressures. *Nat. Sci. Rev.* **2017**, *28*, 121–135.
- 8 Bolz, L. H.; Mauer, F. A.; Peiser, H. S. Exploratory Study, by Low-Temperature X-ray Diffraction Techniques, of Diborane and the Products of a Microwave Discharge in Diborane. *J. Chem. Phys.* **1959**, *31*, 1005–1007.
- 9 Smith, H. W.; Lipscomb, W. N. Single-Crystal X-ray Diffraction Study of β -Diborane. *J. Chem. Phys.* **1965**, *43*, 1060–1064.
- 10 Torabi, A.; Song, Y.; Staroverov, V. N. Pressure-Induced Polymorphic Transitions in Crystalline Diborane Deduced by Comparison of Simulated and Experimental Vibrational Spectra. *J. Phys.*

- 1
2
3 *Chem. C* **2013**, *117*, 2210–2215.
- 4
5 11 Torabi, A.; Murli, C.; Song, Y.; Staroverov, V. N. Polymorphic Transitions of Diborane at Sub-
6 and Near-Megabar Pressures. *Sci. Rep.* **2015**, *5*, 13929.
- 7
8 12 Yao, Y.; Hoffmann, R. BH₃ under Pressure: Leaving the Molecular Diborane Motif. *J. Am.*
9 *Chem. Soc.* **2011**, *133*, 21002–21009.
- 10
11
12 13 Perdew, J. P.; Burke, K.; Ernzerhof, M. Generalized Gradient Approximation Made Simple.
13 *Phys. Rev. Lett.* **1996**, *77*, 3865–3868.
- 14
15
16 14 Perdew, J. P.; Ruzsinszky, A.; Csonka, G. I.; Vydrov, O. A.; Scuseria, G. E.; Constantin, L. A.;
17 Zhou, X.; Burke, K. Restoring the Density-Gradient Expansion for Exchange in Solids and
18 Surfaces. *Phys. Rev. Lett.* **2008**, *100*, 136406.
- 19
20
21 15 Román-Román, E. I.; Zicovich-Wilson, C. M. The Role of Long-Range van der Waals Forces in
22 the Relative Stability of SiO₂-Zeolites. *Chem. Phys. Lett.* **2015**, *619*, 109–114.
- 23
24
25 16 Deringer, V. L.; Stoffel, R. P.; Dronskowski, R. Thermochemical Ranking and Dynamic Stability
26 of TeO₂ Polymorphs from *ab Initio* Theory. *Cryst. Growth Des.* **2014**, *14*, 871–878.
- 27
28
29 17 Whittleton, S. R.; Otero-de-la-Roza, A.; Johnson, E. R. Exchange-Hole Dipole Dispersion Model
30 for Accurate Energy Ranking in Molecular Crystal Structure Prediction. *J. Chem. Theory Com-*
31 *put.* **2017**, *13*, 441–450.
- 32
33
34 18 Hoja, J.; Reilly, A. M.; Tkatchenko, A. First-Principles Modeling of Molecular Crystals: Struc-
35 tures and Stabilities, Temperature and Pressure. *WIREs Comput. Mol. Sci.* **2017**, *7*, e1294.
- 36
37
38 19 Hermann, J.; DiStasio Jr., R. A.; Tkatchenko, A. First-Principles Models for van der Waals
39 Interactions in Molecules and Materials: Concepts, Theory, and Applications. *Chem. Rev.* **2017**,
40 *117*, 4714–4758.
- 41
42
43 20 Zhang, Y.; Yang, W. Comment on “Generalized Gradient Approximation Made Simple”. *Phys.*
44 *Rev. Lett.* **1998**, *80*, 890.
- 45
46
47 21 Grimme, S. Semiempirical GGA-Type Density Functional Constructed with a Long-Range Dis-
48 persion Correction. *J. Comput. Chem.* **2006**, *27*, 1787–1799.
- 49
50
51 22 Grimme, S.; Antony, J.; Ehrlich, S.; Krieg, H. A Consistent and Accurate *ab Initio* Parametriza-
52 tion of Density Functional Dispersion Correction (DFT-D) for the 94 Elements H–Pu. *J. Chem.*
53 *Phys.* **2010**, *132*, 154104.
- 54
55
56 23 Grimme, S.; Ehrlich, S.; Goerigk, L. Effect of the Damping Function in Dispersion Corrected
57 Density Functional Theory. *J. Comput. Chem.* **2011**, *32*, 1456–1465.
- 58
59
60

- 1
2
3 24 Grimme, S.; Hansen, A.; Brandenburg, J. G.; Bannwarth, C. Dispersion-Corrected Mean-Field
4 Electronic Structure Methods. *Chem. Rev.* **2016**, *116*, 5105–5154.
5
6
7 25 Becke, A. D.; Johnson, E. R. Exchange-Hole Dipole Moment and the Dispersion Interaction. *J.*
8 *Chem. Phys.* **2005**, *122*, 154104.
9
10 26 Johnson, E. R.; Becke, A. D. A Post-Hartree–Fock Model of Intermolecular Interactions. *J.*
11 *Chem. Phys.* **2006**, *123*, 024101.
12
13
14 27 Johnson, E. R.; Becke, A. D. A Post-Hartree–Fock Model of Intermolecular Interactions: Inclu-
15 sion of Higher-Order Corrections. *J. Chem. Phys.* **2006**, *124*, 174104.
16
17
18 28 Becke, A. D.; Johnson, E. R. Exchange-Hole Dipole Moment and the Dispersion Interaction
19 Revisited. *J. Chem. Phys.* **2007**, *127*, 154108.
20
21 29 Dion, M.; Rydberg, H.; Schröder, E.; Langreth, D. C.; Lundqvist, B. I. Van der Waals Density
22 Functional for General Geometries. *Phys. Rev. Lett.* **2004**, *92*, 246401.
23
24
25 30 Otero-de-la-Roza, A.; Johnson, E. R. A Benchmark for Non-Covalent Interactions in Solids. *J.*
26 *Chem. Phys.* **2012**, *137*, 054103.
27
28 31 Otero-de-la-Roza, A.; Johnson, E. R. Non-Covalent Interactions and Thermochemistry Using
29 XDM-Corrected Hybrid and Range-Separated Hybrid Density Functionals. *J. Chem. Phys.*
30 **2013**, *138*, 204109.
31
32
33 32 Risthaus, T.; Grimme, S. Benchmarking of London Dispersion-Accounting Density Functional
34 Theory Methods on Very Large Molecular Complexes. *J. Chem. Theory Comput.* **2013**, *9*,
35 1580–1591.
36
37
38
39 33 Perdew, J. P.; Constantin, L. A.; Sagvolden, E.; Burke, K. Relevance of the Slowly Varying
40 Electron Gas to Atoms, Molecules, and Solids. *Phys. Rev. Lett.* **2006**, *97*, 223002.
41
42
43 34 Giannozzi, P.; Baroni, S.; Bonini, N.; Calandra, M.; Car, R.; Cavazzoni, C.; Ceresoli, D.;
44 Chiarotti, G. L.; Cococcioni, M.; Dabo, I. *et al.* QUANTUM ESPRESSO: A Modular and
45 Open-Source Software Project for Quantum Simulations of Materials. *J. Phys. Condens. Matter*
46 **2009**, *21*, 395502.
47
48
49
50 35 Monkhorst, H. J.; Pack, J. D. Special Points for Brillouin-Zone Integrations. *Phys. Rev. B* **1976**,
51 *13*, 5188–5192.
52
53
54 36 Vanderbilt, D. Soft Self-Consistent Pseudopotentials in a Generalized Eigenvalue Formalism.
55 *Phys. Rev. B* **1990**, *41*, 7892–7895.
56
57
58 37 Blöchl, P. E. Projector Augmented-Wave Method. *Phys. Rev. B* **1994**, *50*, 17953–17979.
59
60

- 1
2
3 38 Kresse, G.; Joubert, D. From Ultrasoft Pseudopotentials to the Projector Augmented-Wave
4 Method. *Phys. Rev. B* **1999**, *59*, 1758–1775.
5
6 39 QUANTUM ESPRESSO Pseudopotential Library, [http://www.quantum-
8 espresso.org/pseudopotentials](http://www.quantum-
7 espresso.org/pseudopotentials) (accessed May 22, 2018).
9
10 40 Mattsson, T. R.; Root, S.; Mattsson, A. E.; Shulenburger, L.; Magyar, R. J.; Flicker, D. G.
11 Validating Density-Functional Theory Simulations at High Energy-Density Conditions with
12 Liquid Krypton Shock Experiments to 850 GPa on Sandia’s Z Machine. *Phys. Rev. B* **2014**,
13 *90*, 184105.
14
15 41 Frisch, M. J.; Trucks, G. W.; Schlegel, H. B.; Scuseria, G. E.; Robb, M. A.; Cheeseman, J. R.;
16 Scalmani, G.; Barone, V.; Petersson, G. A.; Nakatsuji, H. *et al. Gaussian 09*, Revision D.01,
17 Gaussian, Inc., Wallingford, CT (2009).
18
19 42 Cammi, R.; Cappelli, C.; Mennucci, B.; Tomasi, J. Calculation and Analysis of the Harmonic
20 Vibrational Frequencies in Molecules at Extreme Pressure: Methodology and Diborane as a
21 Test Case. *J. Chem. Phys.* **2012**, *137*, 154112.
22
23 43 Otero-de-la-Roza, A.; Johnson, E. R. Van der Waals Interactions in Solids Using the Exchange-
24 Hole Dipole Moment Model. *J. Chem. Phys.* **2012**, *136*, 174109.
25
26 44 Pickard, C. J.; Needs, R. J. Structure of Phase III of Solid Hydrogen. *Nat. Phys.* **2007**, *3*,
27 473–476.
28
29 45 Tkatchenko, A.; DiStasio Jr., R. A.; Car, R.; Scheffler, M. Accurate and Efficient Method for
30 Many-Body van der Waals Interactions. *Phys. Rev. Lett.* **2012**, *108*, 236402.
31
32 46 Marom, N.; DiStasio Jr., R. A.; Atalla, V.; Levchenko, S.; Reilly, A. M.; Chelikowsky, J. R.;
33 Leiserowitz, L.; Tkatchenko, A. Many-Body Dispersion Interactions in Molecular Crystal Poly-
34 morphism. *Angew. Chem. Int. Ed.* **2013**, *52*, 6629–6632.
35
36 47 Ambrosetti, A.; Reilly, A. M.; DiStasio Jr., R. A.; Tkatchenko, A. Long-Range Correlation En-
37 ergy Calculated from Coupled Atomic Response Functions. *J. Chem. Phys.* **2014**, *140*, 18A508.
38
39 48 Reilly, A. M.; Tkatchenko, A. Van der Waals Dispersion Interactions in Molecular Materials:
40 Beyond Pairwise Additivity. *Chem. Sci.* **2015**, *6*, 3289–3301.
41
42
43
44
45
46
47
48
49
50
51
52
53
54
55
56
57
58
59
60

TOC Graphic

